Optical Materials 134 (2022) 113133

Contents lists available at ScienceDirect

Optical Materials

journal homepage: www.elsevier.com/locate/optmat

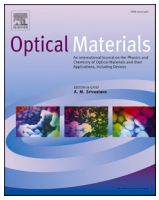

Research Article

Flexible photonics in low stiffness doped silica for use in fibre reinforced polymer composite materials

C. Holmes [a,*], M. Godfrey [b], P.L. Mennea [a], S. Zahertar [a], J.M. Dulieu-Barton [c]

[a] University of Southampton, Optoelectronics Research Centre, Southampton, United Kingdom
[b] University of Southampton, School of Engineering, Southampton, United Kingdom
[c] University of Bristol, Bristol Composites Institute, School of Civil Aerospace and Mechanical Engineering, Bristol, United Kingdom

ARTICLE INFO

Keywords:
Flexible Photonics
Advanced Composites
Planar Optics
Silica
Flame Hydrolysis Deposition

ABSTRACT

The production of a flexible photonic device in doped silica with a Young's modulus that is significantly less than that of traditional silica glass is described. Here the purpose of reducing the modulus is to make planar sensors more applicable for integration into fibre reinforced polymer composite structures. The flexible planar substrate (58 μm thick) consists of three doped silica layers, fabricated using sacrificial silicon wafer processing. It is demonstrated that a Young's modulus of around 40 GPa can be achieved in comparison to a value above 70 GPa for typical silica glass. The optical response of a few mode waveguide that is direct UV written within the central core layer of the flexible glass platform is described. The mechanical stiffness of the platform is determined using nano-indentation tests and confirmed in mechanical tests that demonstrate clearly the flexible nature of the platform. To assess usability for applications integrated into structures undergoing mechanical loading the fatigue lifetime for one million bending cycles is investigated. No degradation to the optical response was observed under the performed testing.

1. Introduction

Integrated optics are conventionally fabricated upon rigid substrates, such as silicon. However, the emerging field of Flexible Photonics is redefining this constraint, offering integrated optics that can uniquely interface with nonplanar, curvilinear, and flexing structures under dynamic loading. The new family of flexible photonic components has been developed on several complementary substrates, comprehensively reviewed in several recent articles [1–5]. Primarily, developments have considered the use of thin flexible polymer substrates [1,6,7], either indirectly through material transfer, where a polymer typically acts as a host [8], or directly utilising the polymer itself [9]. In the latter, optical functionality has been defined through numerous methods including injection moulding, ink-jet printing, screen printing, embossing, and spin coating.

Significant progress in flexible planar glass substrate technology has been made, where the materials are typically noted for their thermal and chemical stability. Flexible soft glasses, including chalcogenides [3,4,6,9,10] and commercialisation of alkali-free borosilicate (Willow Glass from Corning) and aluminosilicate (AS 87 Eco from Schott) have resulted from advances for flexible consumer electronics. For silica-based glasses, developments have included the introduction of waveguiding functionality including use of ultrafast laser direct writing in Willow Glass [11] and rare-earth coatings on AS 87 Eco [12], limitations of ultra-thin alkali-free borosilicate, boroaluminosilicate and sodium aluminosilicate have also been recently reported [13].

One interesting application for flexible photonics is integration into high value fibre-reinforced polymers, e.g., carbon-fibre-reinforced polymer (CFRP) and glass-fibre-reinforced polymer (GFRP). This builds upon decades of development embedding optical fibres into such materials for in-process and structural health monitoring [14–16]. Here flexible photonics offers new functionality to the composite material, associated with planar lightwave circuits. Recent developments have considered silicon planar photonics [17], polymer planar photonics [18–20] and planar fused silica [21] within composites. This work considers flexible multilayer doped planar silica, fabricated through flame hydrolysis deposition (FHD). So far, this substrate has offered new composite material functionality, including an embedded optical switch

Abbreviations: FBG, Fibre Bragg gratings; FHD, Flame Hydrolysis Deposition; GFRP, Glass Fibre Reinforced Polymer; CFRP, Carbon Fibre Reinforced Polymer; FRP, Fibre Reinforced Polymer; SLED, Superluminescent Light Emiiting Diode.

* Corresponding author.
E-mail address: christopher.holmes@soton.ac.uk (C. Holmes).

https://doi.org/10.1016/j.optmat.2022.113133
Received 11 July 2022; Received in revised form 3 October 2022; Accepted 15 October 2022
Available online 5 November 2022

[22] and through thickness strain sensor [23]. FHD doped silica has widely been used for rigid planar lightwave circuits but, as of yet, not a platform for flexible photonics. Hence, to the authors' knowledge the present paper provides the first report, describing FHD silica as a planar flexible substrate and quantification of its physical parameters.

The purpose of this paper is to quantify the Youngs modulus and fatigue lifetime of flexible FHD planar doped silica, embedded in composite materials and used for micromechanical devices [24–29]. As the planar material has a layered composition, the Young's modulus is confirmed using mechanical tests, which also demonstrate the flexibility of the platform. To assess the suitability of integrating a sensor into a loaded structure the effect of mechanical fatigue loading on optical performance is studied.

The next section of the paper describes the materials and fabrication of the sensors, this is followed by a description of the experiments and results in section 3 and a discussion of the results in section 4. Finally some conclusions are presented that highlight the novelty of the work and the important step forward to fabricating sensors that are more mechanically compatible with the fibre reinforced polymer composite materials."

2. Sensor materials and fabrication

The flexible substrate is produced by creating multiple doped layers via FHD [30], which is subsequently removed from a supporting silicon wafer through physical machining. FHD deposition is conducted in three stages to form an underclad, core and overclad. Deposition was made upon a 1 mm thick sacrificial silicon wafer (152 mm diameter, p-doped [1 0 0]). The wafer had a 6 μm thick wet oxide layer, which prevented reaction between the silicon substrate and the deposited doped glass. The underclad and overclad recipes were identical in composition, balancing the stress differentials on either side of the flexible substrate, limiting inherent curvature once released from the sacrificial silicon substrate. The deposited thicknesses of the underclad, core and overclad were 32 μm, 5 μm, 16 μm respectively. Note, the underclad was intentionally made thicker than the overclad to accommodate for any error in the physical machining of the sacrificial silicon substrate beneath. Recipes for the underclad and overclad layers were identical, both flowing $SiCl_4$ at 137 sccm, BCl_3 at 70 sccm and PCl_3 at 31 sccm, through a hydrogen-oxygen flame of flow rate 6.5 l/min (H_2) and 1.5 l/m (O_2). The core was fabricated with flow rates of $SiCl_4$ 123 sccm, $GeCl_4$ 130 sccm, BCl_3 at 16 sccm through a hydrogen-oxygen flame of 5.4 l/min and 2.7 l/min. Each of the three FHD layers were consolidated at high temperature after deposition. The peak temperature of the core layer consolidation was 1,360 °C and 1,250 °C for the cladding layers. As a result of high temperature processing there was dopant diffusion, which increased the core layer thickness to ~9.2 μm. The nominal refractive indices of the individual layers were 1.4452 for the clad layers and 1.4635 for the core at a wavelength of 1553 nm. Indices of refraction and thickness of the three layers were calibrated using a Metricon (Model 2010) prism coupler. This approach required use of individual reference wafers, one for each layer deposited. Measurement of the reference wafers using the Metricon system provided nominal values for the three layers. This did not take into consideration diffusion between dopants in the layers, which is evident by microscopy shown in Fig. 1. As a result of diffusion, the planar waveguide is graded index. Upon deposition of the three glass layers, small spot direct UV laser (SSDUW) writing was used to define a waveguide into the central core layer [31], observable in Fig. 1. The technique can simultaneously define waveguides and Bragg gratings within a UV photosensitive planar glass substrate. Photosensitivity of the central core layer is achieved with localised germanium and boron doping and hydrogenation at a pressure of 120 bar for 10 days and typically achieves propagation losses less than 0.2 dB/cm [32] and insertion loss of 0.2 dB per facet [33]. Waveguides were written [31], with UV laser fluence of 14 $kJcm^{-2}$ (from a 244 nm wavelength, frequency doubled argon ion laser) resulting in a waveguide with a fundamental effective refractive index of 1.45694, calculated directly using the Bragg condition. The resulting waveguide is graded index, horizontally defined by the spotsize of the focused UV laser (1/e ~7 μm) and vertically defined by dopant diffusion between deposited layer.

The final stage of fabrication was removal of the rigid silicon substrate, through a physical machining process. This was initially explored using the top-down approach of wet etching. However, it was observed that large stress differentials of the order 150 MPa [34] caused mechanical failure of the silica when the thickness of the silicon approached that of the silica glass. To overcome this, a raster scan dicing approach was developed that removed all the silicon incrementally. The physical machining (dicing) was achieved using a resin bonded diamond impregnated blade (DISCO R07-SD1200 series), with a 250 μm kerf blade with a spindle speed of 25,000 RPM and feedrate of 5 mm s^{-1}. Firstly, the machining process was used to dice the chips to size. The chosen chip dimension for the work described in the following sections of the paper was 1 mm × 60 mm. After this step the silicon was removed from the underside using a raster cut process, with a period of 90 μm. The physical machining process resulted in a small undulation on one side of the substrate, resulting from the form of the saw blade (radius of blade tip ~125 μm). These features could be removed through lapping/polishing.

3. Experimental arrangements and results

The following section describes approach taken and results for measuring the Youngs Modulus, hardness and density of the flexible photonic substrate and measurement approach for fatigue lifetime.

3.1. Mechanical properties

The density of the FHD formed glass was obtained by using a top pan balance (Sartorius Genius) to measure the mass and a microscope to determine the glass sample dimensions, which were confirmed with a stylus profiler (Tencor P60+). The measured density of 1.84 ± 0.09 g cm^{-3} is 16% lower than reported values of 2.202 g cm^{-3} for fused silica.

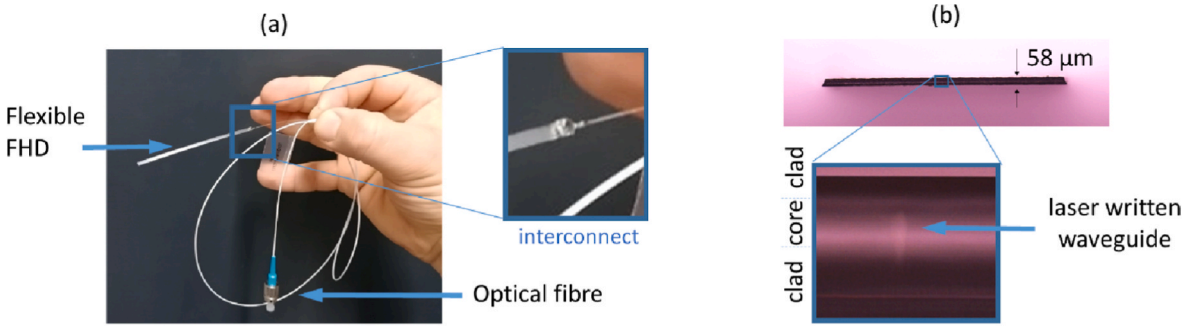

Fig. 1. Flexible doped silica substrate (a) connected to an optical fibre, (b) a micrograph showing a cross section of the multilayers and laser written waveguide.

The reduced density indicates strongly that the FHD formed glass will not have similar mechanical properties to that of silica glass. For integration/embedding into laminated composite structure it would be beneficial for the FHD formed glass to have a reduced Young's modulus as this would reduce any local stiffening of the structure. Therefore, it is necessary to determine the Young's modulus of FHD formed glass to assess any local stiffening effects of the platform. Firstly, the Young's modulus was obtained using nano-indentation tests and compared with typical materials. To confirm the results, a three-point bending test was undertaken, which also serves to demonstrate the flexibility of the FHD formed glass.

3.1.1. Nano-indentation measurements

Nanoindentation enables an experimental determination of Young's modulus independently of substrate thickness. With this technique, it was also possible to quantify glass hardness.

Three samples were studied: (i) 'FHD on Silicon': multi-layered doped silica deposited on a thick sacrificial silicon substrate using FHD, i.e. prior-to-machining, (ii) 'Diced FHD': the FHD formed 'flexible glass' material, i.e. after machining, and (iii) 'Drawn Fused Silica': as a control, a drawn fused silica sample with an expected Youngs Modulus to be equivalent to that of fused silica [35]. The equipment used for the nano-indentation tests was a Nano Test Vantage instrument (Micro Materials Ltd., Wrexham, UK). The experiments were conducted in load control with a Berkovich diamond. An indentation load of 150 mN was used, with a range of loads from 50 mN to 350 mN with 50 mN increments for the FHD on silicon sample to establish hardness and Young's modulus as a function of depth. At least 8 indentions were used for each sample, where adjacent indents were separated by 30 μm, apart from the flexible glass, where the separation was increased to 100 μm due to the higher loads of some of the indents for the depth profile experiment. The samples and loading conditions are outlined in Table 1.

The hardness and reduced moduli were extracted using power law fitting between 100% and 20% of the unloading curve using the Oliver Pharr method [36]. A dwell time of 10 s was used at maximum load to minimise the influence of creep and the system was corrected for thermal drift and frame compliance. Both the loading and unloading times were set to 15 s.

As described by the Bückle rule, the interaction volume is approximately 10 times the indentation depth [37]. For the samples that experienced an indentation force of 150 mN, the depth was between 1 and 1.5 μm; therefore, the properties were measured over the first 10–15 μm of glass – i.e., approximately 20–37% of the total thickness of the glass. In the load profile experiment, the interaction depth was about 21 μm at 350 mN load, which is approximately half of the glass thickness. This was decided as the best compromise in force because the indenter was interacting with the bulk of the glass (minimising any skin effects), whilst not interacting with the silicon substrate, or glass near the silicon. It must be noted that between the extremes in indentation force (50 and 350 mN), the Young's Modulus varied by around 10%, which shows the measured stiffness is a relatively weak function of indentation force.

Table 1
The samples and conditions for nanoindentation tests.

Sample Name	Sample Description	Indentation Loads (mN)	Indent Separation (μm)
FHD on Silicon	Multi-layered doped silica deposited on a thick silicon substrate using FHD.	50, 100, 150, 200, 250, 300, 350	100
Diced FHD	Identical to 'FHD on Silicon' but with the silicon substrate removed by machining.	150	30
Drawn Fused Silica	Drawn fused silica with an expected Youngs Modulus to be equivalent to that of fused silica.	150	30

Fig. 2 (a) shows the hardness value against indentation force for the FHD material on the silicon substrate. It is seen that as the indentation force increases for the flexible substrate, the hardness increases. This is likely due to higher residual compressive stress nearer the silicon substrate [38,39]. The conversion to Young's modulus, E, is described by the following equation [40]:

$$E = \frac{(1-\nu^2)}{\frac{1}{E_r} - \frac{1-\nu_i^2}{E_i}} \tag{1}$$

where ν is Poisson's ratio and the subscript i refers to the indenter diamond ($E_i = 1141$ GPa, $\nu_i = 0.07$) [40].

Fig. 2 (b) shows a plot the Young's modulus derived from equation (1) against indentation force, assuming a Poisson's ratio of 0.17 [40]; as expected the Young's modulus increases as hardness increases. Fig. 2 (c)–(d) summarise the stiffness and hardness values captured for all three materials. The drawn fused silica provides the greatest Young's modulus of 71.3 GPa practically identical to that of fused silica (i.e., 71.2 GPa [41]). This confirms the validity of the nanoindentation procedure adopted here and indicates that the assumed value of Poisson's ratio is valid. The FHD glass when attached to the silicon wafer exhibited a higher modulus of 46.9 GPa compared to 40.0 GPa for the FHD formed glass with the silicon removed. This is likely due to compressive residual stress in the glass layer due to the silicon substrate [38].

There may be some error in deriving the Young's modulus from equation (1) because of the approximation of the material Poisson's ratio, which could be different from the value quoted in Ref. [28] for the FHD formed glass. A greater source of error may be the layered nature of the FHD material; hence it was decided to conduct some mechanical tests to estimate the Young's modulus of the FHD formed glass with the silica removed, which is independent of Poisson ratio.

3.1.2. Mechanical flexure

A strip of the FHD formed glass material of dimensions (60 mm by 2 mm by 47 μm) was cut for the mechanical flexure tests. An accurate measurement of the thickness was required due to the cubic relationship of the second moment of area and thickness. Therefore, three measurement methods were used to calibrate, namely a micrometer, graticule calibrated optical microscope and stylus profiler (KLA Tencor P16+), to corroborate thickness value to within 5 μm. For the flexural tests the optical fibre connection was not made to the chip nor and direct laser written waveguide or Bragg gratings, to ensure the adjoining fibre did not influence the measurements. A three-point bending rig was mounted in an Instron Electropuls electrodynamic test machine (see Fig. 3 (a)), The rig comprised a base section with two roller supports of 6 mm diameter positioned 30 mm apart and an upper section that was fitted to the upper clamp in the test machine. As the loads to deform the FHD material were predicted to be very small, a top pan balance that had a sensitivity of 10 mg was positioned between the base of the rig and the base of the machine, as shown in Fig. 3 (a). This enabled the load to be applied in displacement control with the balance recording the load with greater fidelity than could be achieved with the 1 kN load cell that was fitted to the test machine. In this arrangement the flexural modulus E_f is calculated using

$$E_f = \frac{PL^3}{48dI} \tag{2}$$

Where d is the displacement of the central roller, P is the applied load, L is the support span, I is the second moment of area and E is the Young's modulus.

The mechanical response is shown in Fig. 3 (b). It should be noted that after 4 mm of displacement the glass beam exhibits a non-linear force-displacement profile.

The Young's modulus was calculated from equation (2) using the

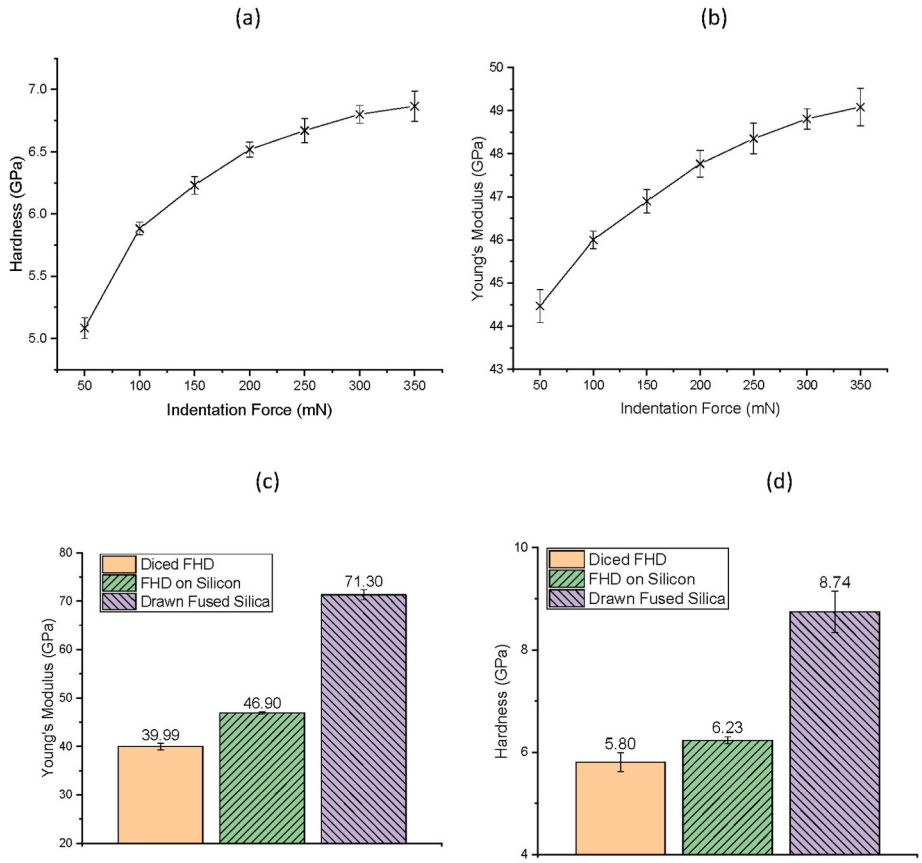

Fig. 2. Nano-indentation data, showing (a) Hardness and (b) Young's Modulus as a function of indentation Force for the silica-on-silicon platform and the summarised (c) Young's Modulus and (d) hardness values for silica substrate bonded to sacrificial silicon, with silicon machined away (i.e., flexible) and control fused silica sample drawn on an optical fibre drawing tower.

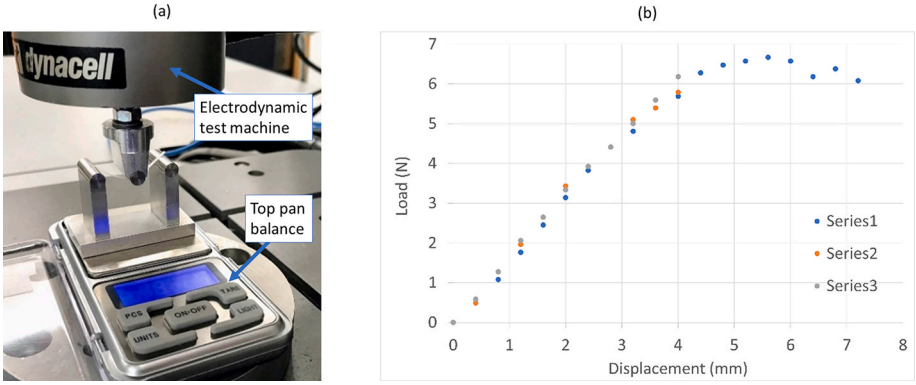

Fig. 3. Stiffness measurement of flexible doped silica substrate subject to 3-point bending, (a) the experimental arrangement (b) measured load for varying displacement over three repeated tests.

mean of linear gradient repeats shown in Fig. 3 (b). This provided a result of 50 ± 10 GPa, which was within the error of that derived through nanoindentation measurement, 40.0 ± 0.7 GPa. These values are lower than previously reported values for pure bulk silica fabricated through FHD (72.4 GPa) [42]. Fig. 4 is an Ashby plot, showing the difference in density and Young's modulus of flexible FHD compared to flexible commercial glass (Corning Willow, AGC Spool, NEG G-Leaf and Schott AF32) [5] and bulk fused silica and borosilicate. Flexible FHD has notable differentiation with commercial glass families and interestingly closer to the Young's modulus of some unidirectional Fibre Reinforced Polymers (FRPs) in the fibre direction [43], making this glass potentially more suitable for embedded strain sensors due to the likelihood of an even strain distribution in and around the sensor.

Evident form Fig. 4, the flexible FHD has a lower measured density 1.84 g cm^{-3} compared to previous reports for FHD glass of 2.156–2.206 g/cm^3 [42,44,45]. The relatively low density values could be an indication of incomplete consolidation, a feature also suggested in recent work investigating microwave consolidation [46]. To explore this further a scanning electron microscope (SEM) was used to image the glass surfaces, shown in Fig. 5.

FHD soot consolidation is well understood [47,48], as a uniform agglomeration of well-defined small particles, they pack together very densely upon a temperature increase until there are no marked grains. For substrate temperatures of 200 °C (conditions used in this work)

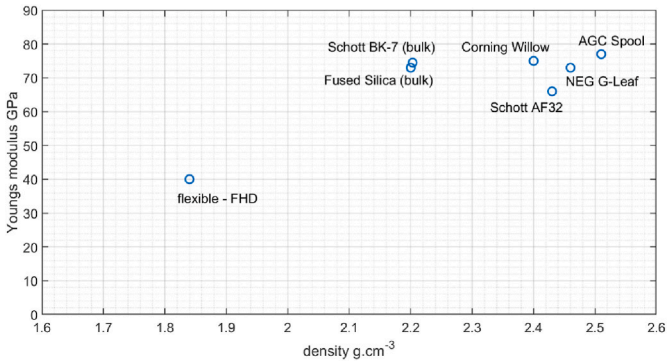

Fig. 4. An Ashby plot showing the physical properties of commercial flexible glass, bulk glass (fused silica and borosilicate) and flexible FHD.

initial particle sizes are ~100 nm [45]. From Fig. 5, the cleaved side edge is most indicative of the internal glass matrix. It shows no obvious voids at this scale and so it is assumed full consolidation has been made. It is therefore unlikely that the density anomaly arises from partial consolidation.

3.2. Fatigue lifetime measurement

For practical applications it is essential to validate fatigue lifetime. Fatigue lifetime measurements were achieved here by conducting a 1,000,000 cycle 3-point bend test using an Instron E10000 test machine with the same set-up as described previously. The separation of the bottom two supports was 30 mm and the deflection of the central top pivot was 2 mm, at frequency of 1 Hz. For these tests a new flexible substrate was fabricated. As the sample was unique the test methodology was designed specifically for this study. Recourse to standards for mechanical testing was not considered to be necessary, as a large deformation was required to maximise any spectral response from flexure. The lower roller separation was made as large as reasonably possible, limited by the sample size.

Light was coupled into the flexible substrate using butt coupled single mode polarisation maintaining optical fibre, secured with UV-cured optical adhesive (Dymax OP4-20632). The stress rods in the optical fibre were aligned parallel to the core layer by using a microscope to end view the optical fibre, this permitted separate interrogation of optical polarisation states. The fabricated gratings were 12 mm in length and had uniform apodisation profile.

Prior to the fatigue test the thermo-optic response was calibrated, by cooling the device in a dewar flask and logging its temperature using a K-type thermocouple as it increased back to room temperature. The measured response was 11.5 ± 0.1 p.m./K for transverse electric (TE) and 11.1 ± 0.1 p.m./K for transverse magnetic (TM) fundamental modes (made over a 40 °C temperature range). These measurements were separately taken, and the polarisation state selected using an in-line fibre polariser. The spectral birefringence at room temperature was

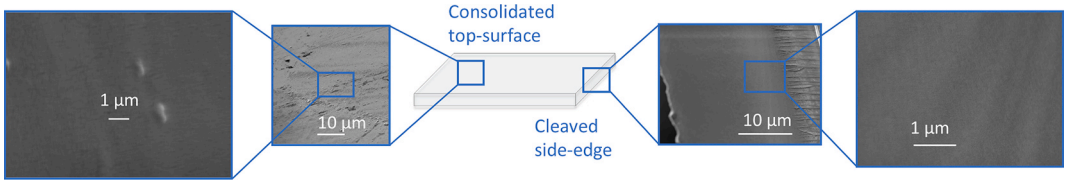

Fig. 5. Scanning Electron Micrographs showing the top face and cleaved edge.

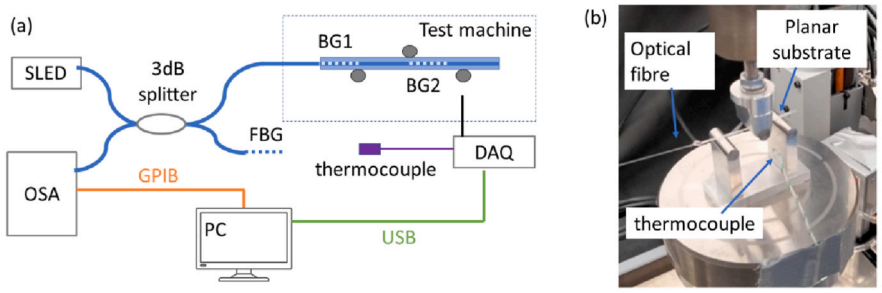

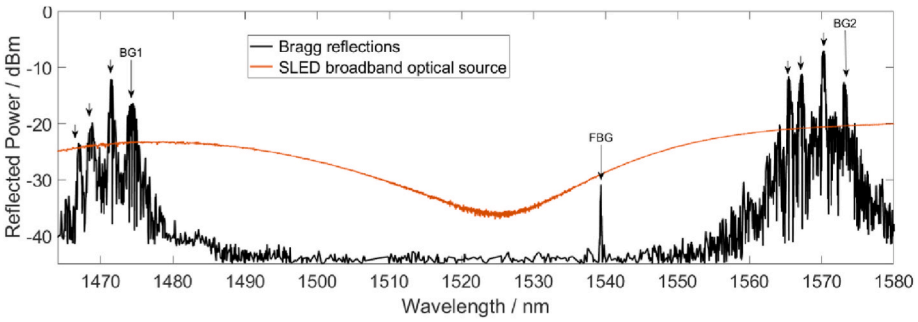

Fig. 6. The fatigue test set-up showing (a) schematic of the experimental set-up and (b) a photograph of the loaded flexible FHD under 3-point bending (c) spectral signature of Bragg gratings, showing fundamental and higher order modes of BG1 and BG2 and broadband optical source (Fresnel reflection from single arm of the 3 dB splitter).

measured to be 25 p.m.

Fig. 6 (a) and (b) illustrate the fatigue test set-up. Actuation was paused every 200 cycles (3 min 20 s) and the spectra captured, an example spectra is shown in Fig. 6 (c). Three multiplexed Bragg gratings were recorded, two on the flexible substrate (BG1 and BG2 of grating period 505.94 nm and 539.81 nm respectively) and one in GF4A optical fibre (FBG of grating period 529.38 nm). Drift in polarisation state was minimised during test by clamping all non-polarisation maintaining optical fibre to laboratory benches. In addition to the spectra the laboratory temperature was logged with a K-type thermocouple.

Fig. 7 shows the power reflected by the Bragg gratings, *A*, relative to the average reflected power, over one million load cycles. It should be noted that data collection was not continuous. During the 1,000,000 cycles (totalling over 11.5 days), the system unexpectedly stopped 160,000 cycles into testing (~2 days). Here a discrete decrease in reflected power can be seen for BG2 (Fig. 7 (b)) and the FBG (Fig. 7 (c)), whereas there is an increase in reflected power for BG1 (Fig. 7 (a)). It should be noted that the SLED source contains multiple SLEDs, to provide its broadband coverage. The Bragg gratings do not reflect light from the same SLED, namely BG1 reflects light from a different SLED within the source, shown in Fig. 6 (c). Drift in the individual sources is considered to be the reason for the increase in amplitude after cycle 160,000 for BG1 and a decrease in amplitude for the FBG and BG2 (both of which share the same SLED).

All amplitude variations can be attributed to long-term source drift, as the FBG is used as an amplitude reference. The FBG does not undergo any actuation, but exhibits a small variation of amplitude, explained by long-term source drift in the optical interrogation system.

The drift in reflected power is minimal for all Bragg gratings. BG1 and BG2 decrease 0.07 dB and 0.20 dB respectively, FBG increase in 0.06 dB BG1 and BG2 do increase 0.05 and 0.03 dB before 160,000 FBG increase by 0.04 dB.

Fig. 8 shows Bragg shift of all gratings, over one million cycles. There is no significant shift in Bragg wavelength, Fig. 8 (a) and (b) show a similar response to Fig. 8 (c). Spectral variation can primarily be attributed to temperature changes of the lab.

It should be noted that there are small discrepancies between Bragg gratings on the flexible substrate, the reference FBG and the thermocouple. This is likely a result of spatial position in the laboratory and not considered significant after 1,000,000 cycles.

4. Discussion

The Young's modulus and hardness values of the reported flexible FHD substrate are notably lower than previous reports of bulk flame hydrolysis silica. For example, nano-indentation on optical fibre preforms, examining the properties of the gemanosilicate cores, reported a Young's modulus of 74.5 ± 1 GPa and hardness 10.5 ± 0.5 GPa [49]. Another report on pure bulk silica fabricated through FHD and measured using Brillouin spectroscopy showed a Young's modulus of 72.2 GPa [42]. The Young's modulus obtained from the flexible FHD described here is much lower than both these values. Likewise, the density is much lower than previously reported for consolidated flame hydrolysis silica of between 2.156 and 2.206 g/cm^3 [42,44,45]. The lower density and Young's modulus measurements are related, and could be attributed to partial consolidation. However, there are no obvious voids observed in the glass in SEM micrographs ruling out partial consolidation as an explanation for lower density. The main differences between flexible-FHD and previous reports is the deposition upon a thick silicon substrate. As the sacrificial silicon substrate is over an order of magnitude thicker than the FHD being deposited, it is expected to have mechanical influence during the consolidation process. The exact physical mechanism resulting is not yet fully understood and shall be the subject of future investigations.

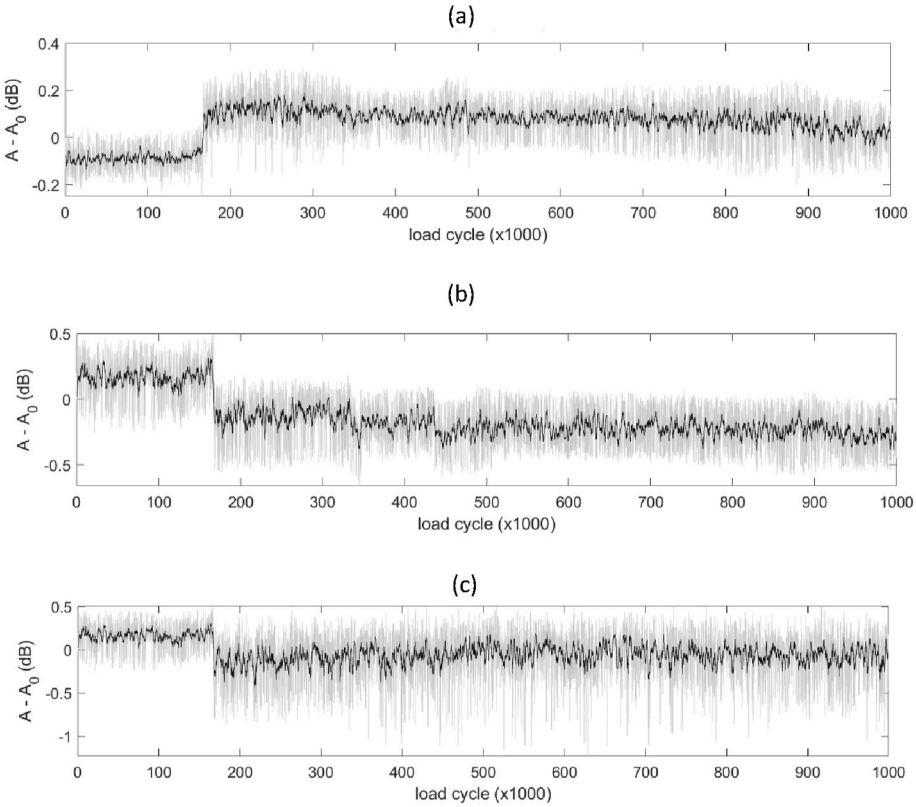

Fig. 7. Relative amplitude change in systems three Bragg gratings, showing (a) BG1 and (b) BG2 and (c) FBG reference (grey line is raw data, black line is a ten-point moving average).

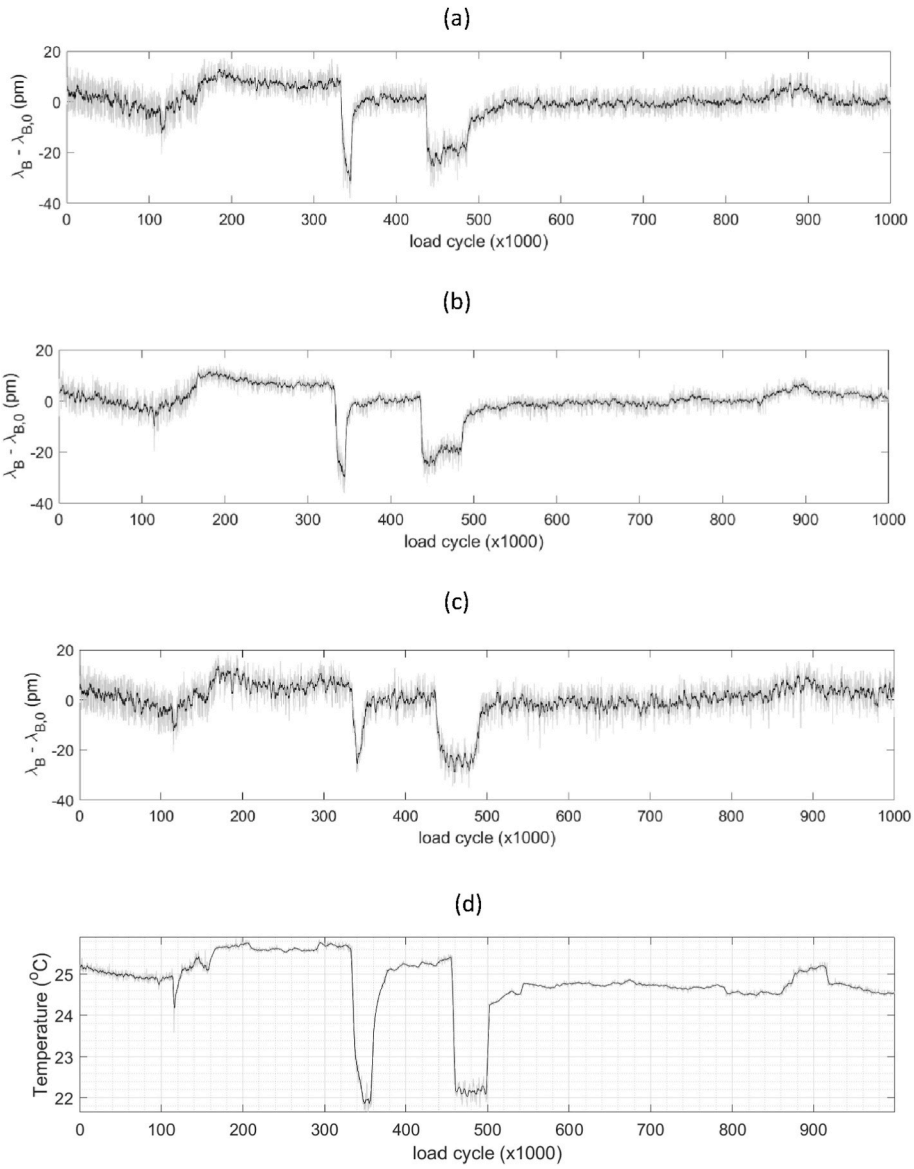

Fig. 8. Fatigue testing of the flexible platform, showing spectral response after 3-point bend actuation for (a) BG1 and (b) BG2 referenced to response of (c) FBG and (d) thermocouple (grey line is raw data, black line is a ten-point moving average).

5. Conclusions

The present paper is the first report of FHD doped silica as a substrate for flexible planar photonics. A quantitative mechanical investigation has observed a lower-than-expected Young's modulus (40.0 ± 0.7 GPa), confirmed through both bending and nanoindentation tests. This is 45% less stiff than fused silica and highlights an interesting mechanical property for flexible photonic integration, particularly in Fibre Reinforced Polymers that can have a lower Youngs Modulus to that of fused silica. The platform showed negligible optical and mechanical degradation after a one million cycle fatigue test showing practical feasibility as a future flexible photonics substrate.

6. Future work

Applications for this flexible photonic glass could include integration into high strain compliant structures/mechanisms, biomedical applications (e.g., monitoring artificial bone, instrumented prosthetics, monitoring artificial tissue/cartilage), use in flexible displays and alongside flexible electronics.

Future work shall explore both the influence of the substrate and the consolidation process upon the mechanical properties of the FHD.

CRediT authorship contribution statement

C. Holmes: Conceptualization, Data curation, Funding acquisition, Project administration, Resources, Supervision, Validation, Methodology, Visualization, Roles, Writing – original draft, Writing – review & editing, Formal analysis, Investigation, Software. **M. Godfrey:** Validation, Methodology, Visualization, Roles, Writing – original draft. **P.L. Mennea:** Investigation, Software. **S. Zahertar:** Investigation. **J.M. Dulieu-Barton:** Validation, Methodology, Visualization, Roles, Writing – original draft, Writing – review & editing.

Declaration of competing interest

The authors declare that they have no known competing financial interests or personal relationships that could have appeared to influence the work reported in this paper.

Data availability

Dataset available DOI https://doi.org/10.5258/SOTON/D2424

Acknowledgements

The authors would like to thank: Dr Richard Cook for his considerable help with the nanoindentation experiments; Prof Francesco Poletti, Dr Thomas Bradley, Mr Nicholas White and Mr Glenn Topley for assistance with flat fibre drawing. The research has been developed under EPSRC 'Roll-2-Roll (R2R) manufacture of multilayer planar optics', EP/V053213/1 and 'EPSRC Future Composites and Manufacturing Hub', EP/P006701/1. For the purpose of open access, the author has applied a creative commons attribution (CC BY) licence (where permitted by UKRI, 'open government licence' or 'creative commons attribution no-derivatives (CC BY-ND) licence' may be stated instead) to any author accepted manuscript version arising.

References

[1] S. Geiger, J. Michon, S. Liu, et al., Flexible and stretchable photonics: the next stretch of opportunities, ACS Photonics 7 (10) (2020) 2618–2635.
[2] W. Peng, H. Wu, Flexible and stretchable photonic sensors based on modulation of light transmission, Adv. Opt. Mater. 1900329 (2019) 1–27.
[3] L. Li, H. Lin, J. Michon, et al., A new twist on glass: a brittle material enabling flexible integrated photonics, Int. J. Appl. Glass Sci. 8 (1) (2017) 61–68.
[4] J. Hu, L. Li, H. Lin, P. Zhang, W. Zhou, Z. Ma, Flexible integrated photonics: where materials, mechanics and optics meet, Opt. Mater. Express 3 (9) (2013) 1313.
[5] G.C. Righini, J. Krzak, A. Lukowiak, G. Macrelli, S. Varas, M. Ferrari, From flexible electronics to flexible photonics: a brief overview, Opt. Mater. 115 (2021) 925–3467.
[6] L. Li, H. Lin, S. Qiao, et al., Integrated flexible chalcogenide glass photonic devices, Nat. Photonics 8 (8) (2014) 643–649.
[7] R. Bruck, P. Muellner, N. Kataeva, et al., Flexible thin-film polymer waveguides fabricated in an industrial roll-to-roll process, Appl. Opt. 52 (19) (2013) 4510–4514.
[8] L. Fan, L.T. Varghese, Y. Xuan, J. Wang, B. Niu, M. Qi, Direct fabrication of silicon photonic devices on a flexible platform and its application for strain sensing, Opt Express 20 (18) (2012), 20564.
[9] J. Missinne, N. Teigell Benéitez, M.A. Mattelin, et al., Bragg-grating-based photonic strain and temperature sensor foils realized using imprinting and operating at very near infrared wavelengths, Sensors 18 (8) (2018) 1–14.
[10] L. Li, H. Lin, S. Qiao, et al., Monolithically integrated stretchable photonics, Light Sci. Appl. 7 (2) (2018), 17138.
[11] S. Huang, M. Li, S.M. Garner, M. Li, K.P. Chen, Flexible photonic components in glass substrates, Opt Express 23 (17) (2015).
[12] K.M. Tan, M. Mazilu, T.H. Chow, et al., In-fiber common-path optical coherence tomography using a conical-tip fiber, Opt Express 17 (4) (2009) 2375.
[13] G. Macrelli, A.K. Varshneya, J.C. Mauro, Ultra-thin glass as a substrate for flexible photonics, Opt. Mater. 106 (May) (2020), 109994.
[14] G. Luyckx, E. Voet, N. Lammens, J. Degrieck, Strain measurements of composite laminates with embedded fibre bragg gratings: criticism and opportunities for research, Sensors 11 (1) (2011) 384–408.
[15] K.S.C. Kuang, R. Kenny, M.P. Whelan, W.J. Cantwell, P.R. Chalker, Embedded fibre Bragg grating sensors in advanced composite materials, Compos. Sci. Technol. 61 (10) (2001) 1379–1387.
[16] S. Minakuchi, N. Takeda, Recent advancement in optical fiber sensing for aerospace composite structures, Photonic Sensors 3 (4) (2013) 345–354.
[17] C. Zervos, G. Poulopoulos, J. Missinne, M. Szaj, H. Avramopoulos, Miniaturized Silicon Photonics Multi-Sensor Operating at High Temperatures for Use in Composite Materials Industrial Applications, 2022, p. 42.
[18] J. Missinne, N. Teigell Benéitez, A. Lamberti, et al., Thin and flexible polymer photonic sensor foils for monitoring composite structures, Adv. Eng. Mater. 20 (6) (2018).
[19] S. Kefer, T. Sauer, S. Hessler, M. Kaloudis, R. Hellmann, Microstructure-based fiber-to-chip coupling of polymer planar bragg gratings for harsh environment applications, Sensors 20 (19) (2020) 1–12.
[20] S. Kefer, T. Sauer, S. Hessler, M. Kaloudis, B. Schmauss, R. Hellmann, Robust polymer planar bragg grating sensors embedded in commercial-grade composites, Polymers 12 (3) (2020) 1–12.
[21] F. Anelli, A. Annunziato, A. Erario, C. Holmes, C. Ciminelli, F. Prudenzano, Design of Microstructured Flat Optical Fiber for Multiaxial Strain Monitoring in Composite Materials; Design of Microstructured Flat Optical Fiber for Multiaxial Strain Monitoring in Composite Materials, 2022.
[22] C. Holmes, M. Godfrey, P.L. Mennea, D.J. Bull, J.M. Dulieu-Barton, Optical switching in glass fibre composite, Journal of Optics and Laser Technology (2022) 152.
[23] C. Holmes, M. Godfrey, D.J. Bull, J. Dulieu-Barton, Real-time through-thickness and in-plane strain measurement in Carbon Fibre Reinforced Polymer composites using planar optical Bragg gratings, Opt Laser. Eng. 133 (106111) (2020).
[24] P.A. Cooper, L.G. Carpenter, P.L. Mennea, C. Holmes, J.C. Gates, P.G.R. Smith, Integrated optical dual-cantilever arrays in silica on silicon, Opt Express 22 (26) (2014).
[25] C. Holmes, L.G. Carpenter, H.L. Rogers, J.C. Gates, P.G.R. Smith, Quantifying the optical sensitivity of planar Bragg gratings in glass micro-cantilevers to physical deflection, J. Micromech. Microeng. 21 (3) (2011).
[26] P.A. Cooper, L.G. Carpenter, C. Holmes, C. Sima, J.C. Gates, P.G.R. Smith, Power-efficiency enhanced thermally tunable bragg grating for silica-on-silicon photonics, IEEE Photonics J 7 (2) (2015) 1–11.
[27] C. Holmes, J.C. Gates, P.G.R. Smith, Integrated optical differential pressure transducers achieved using thin buckled silica membranes and direct UV written planar Bragg gratings, Sens Actuators A Phys 168 (2011) 14–21.
[28] C. Holmes, L.G. Carpenter, J.C. Gates, P.G.R. Smith, Miniaturization of Bragg-multiplexed membrane transducers, J. Micromech. Microeng. 22 (2) (2012), 025017.
[29] L.G. Carpenter, C. Holmes, H.L. Rogers, P.G.R. Smith, J.C. Gates, Integrated optic glass microcantilevers with Bragg grating interrogation, Opt Express 18 (22) (2010) 23296–23301.
[30] P. Tandon, H. Boek, Experimental and theoretical studies of flame hydrolysis deposition process for making glasses for optical planar devices, J. Non-Cryst. Solids 317 (3) (2003) 275–289.
[31] C. Holmes, J.C. Gates, L.G. Carpenter, et al., Direct UV-written planar Bragg grating sensors, Meas. Sci. Technol. 26 (11) (2015), 112001.
[32] H.L. Rogers, S. Ambran, C. Holmes, P.G.R. Smith, J.C. Gates, In situ loss measurement of direct UV-written waveguides using integrated Bragg gratings, Opt Lett 35 (17) (2010) 2849–2851.
[33] D. Zauner, K. Kulstad, J. Rathje, M. Svalgaard, Directly UV-written silica-on-silicon planar waveguides with low insertion loss, Electron. Lett. 34 (16) (1998) 1582–1584.
[34] C. Holmes, P.A. Cooper, H.N.J. Fernando, et al., Direct UV written planar Bragg gratings that feature zero fluence induced birefringence, Meas. Sci. Technol. 26 (12) (2015), 125006.
[35] A.S. Webb, F.R.M. Adikan, JayantaK. Sahu, et al., MCVD planar substrates for UV-written waveguide devices, Electron. Lett. 43 (9) (2007) 1–2.
[36] W.C. Oliver, G.M. Pharr, An improved technique for determining hardness and elastic modulus using load and displacement sensing indentation experiments, J. Mater. Res. 7 (6) (1992) 1564–1583.
[37] H. Bückle, Mikrohärteprüfung Und Ihre Anwendung", Berliner Union, 1965.
[38] K.O. Kese, Z.C. Li, B. Bergman, Influence of Residual Stress on Elastic Modulus and Hardness of Soda-Lime Glass Measured by Nanoindentation, 2004.
[39] Ernsberger, F.M.: "Elastic Properties of Glasses"1980, pp. 1–19.
[40] D.J. Shuman, A.L.M. Costa, M.S. Andrade, Calculating the elastic modulus from nanoindentation and microindentation reload curves, Mater. Char. 58 (4) (2007) 380–389.
[41] T.H. Laby, G.W.C. Kaye, Tables of Physical & Chemical Constants", sixteenth ed., Longman, 2005.
[42] G. Scannell, A. Koike, L. Huang, Structure and thermo-mechanical response of TiO2-SiO2 glasses to temperature, J. Non-Cryst. Solids 447 (2016) 238–247.
[43] D.U. Shah, Natural fibre composites: comprehensive Ashby-type materials selection charts, Mater. Des. 62 (2014) 21–31.
[44] K. Tsukuma, T. Akiyama, High temperature viscosity of nitrogen modified silica glass, J. Non-Cryst. Solids 265 (3) (2000) 199–209.
[45] H. Shin, J.-H. Yi, J.-G. Baek, M. Choi, Preparation and Characterization of SiO 2-B 2 O 3-P 2 O 5 Particles and Films Generated by Flame Hydrolysis Deposition for Planar Light-Wave Circuits, 2002.
[46] C. Holmes, J.C. Gates, P.C. Gow, P.G.R. Smith, Q.S. Ahmed, Microwave consolidation of UV photosensitive doped silica for integrated photonics, Opt. Mater. Express 11 (Issue 6) (2021) 1835–1841, 11, (6), pp. 1835–1841.
[47] C.-G. Choi, M.-Y. Jeong, T.-G. Choy, Characterization of borophosphosilicate glass soot fabricated by flame hydrolysis deposition for silica-on-silicon device applications, J. Mater. Sci. 34 (1999) 6035–6040.
[48] P. Tandon, H. Boek, Experimental and theoretical studies of flame hydrolysis deposition process for making glasses for optical planar devices, J. Non-Cryst. Solids 317 (3) (2003) 275–289.
[49] R. Aashia, K.V. Madhav, U. Ramamurty, S. Asokan, Nanoindentation study on germania-doped silica glass preforms: evidence for the compaction-densification model of photosensitivity, Opt Lett 34 (16) (2009) 2414.